

Pilot Study on Indoor Flows and Turbulence Statistics of a Vertical Axis Wind Turbine

YinMun H'ng¹, Yusri Yusup¹, H. P. S. Abdul Khalil¹ & TjoonTow Teng¹

¹ School of Industrial Technology, Universiti Sains Malaysia, Penang, Malaysia

Correspondence: Yusri Yusup, School of Industrial Technology, Universiti Sains Malaysia, Penang 11800, Malaysia. Tel: 60-4-653-5201. Fax: 60-4-657-3678. E-mail: yusriy@usm.my

Received: March 5, 2014 Accepted: March 25, 2014 Online Published: May 5, 2014

doi:10.5539/mer.v4n1p63

URL: <http://dx.doi.org/10.5539/mer.v4n1p63>

Abstract

Turbulence statistics were applied to the downwind flow of a Darrieus-type vertical axis wind turbine (VAWT) to provide insights about VAWT micro-flow characteristics. Micro-turbulence measurements of the flow in front of and behind a VAWT were made using a sonic anemometer. Turbulence data for downwind distances of 0.5 m and 2.0 m from the wind source were collected with and without the VAWT, respectively, using a blower (Type 1 flow) and industrial fans (Type 2 flow) as the wind source. The voltage V , generated by the VAWT was recorded every 15 min. Only the center line of the flow was considered. The Type 2 flow induced a constant spectral power at a high dimensionless frequency range of $0.007 < f < 0.04$, perhaps due to the fan configuration, which had a larger wind-swept area. The results show an increase in lateral turbulence, σ_v , downwind of the VAWT compared to its longitudinal, σ_u , and vertical, σ_w , counterparts. Using spectral analysis, the VAWT was found to reduce the horizontal (u and v) turbulent component energies in the dimensionless frequency range of 0.003–1. Interesting dip and peak features were observed for Type 1 flow, but only dip features were observed for Type 2 flow in the resulting spectra. Higher wind speeds increased the voltage generated at a rate of 0.5.

Keywords: VAWT, micro-turbulence, spectral power, dimensionless frequency, voltage

1. Introduction

1.1 Darrieus-Type VAWT

There are two types of vertical axis wind turbines (VAWTs): 1) Darrieus and 2) Savonius. The Darrieus VAWT is a lift-type turbine of which the aerodynamic characteristics are similar to a helicopter blade. The vertical airfoil-shaped blades move forward into oncoming wind, producing small but changing positive angles of attack on the blades. This creates a net lift force on the blade, inducing it toward the wind turbine mast and resulting in a positive torque on the shaft. When the wind flows across the VAWT blades, a positive torque is produced; a small or negative torque is produced when the blades spin parallel to the wind.

VAWTs are omnidirectional, which means they do not need to be positioned into the main wind direction and are able to capture winds from any direction (Paulides, Encica, Jansen, Lomonova, & Van Wijck, 2009; Stankovic, Campbell, & Harries, 2009; Stitt, 1999). Thus, they are well suited for areas where the winds are directionally unpredictable. VAWT are increasingly common in the wind energy market, especially for domestic or small scale installations, such as on rooftops and in urban and suburban locations. Moreover, VAWTs are smaller than the traditional horizontal axis wind turbines, so they can be easily integrated onto buildings. Placing a VAWT at a higher elevation such as on a rooftop, provides access to stronger winds with greater mechanical energy. The Darrieus VAWT exhibits an inherent “torque ripple” caused by the continuously changing angles of attack between the turbine blades and the wind (Eriksson, Bernhoff, & Leijon, 2008); torque ripple is defined as the amount of torque measured by subtracting the minimum torque from the maximum torque in one revolution.

Horizontal axis wind turbines are self-starting unlike some VAWTs, which depend on wind conditions. However, the lift-driven VAWT can self-start and operate in low wind speed conditions. When required, an induction motor, which must be connected to its own energy source, is employed to ensure the start-up of the VAWT.

Winds are generally turbulent in the built urban environment (Christen, Rotach, & Vogt, 2009; Rotach et al., 2005; Roth, 2000). Although studies of urban canopy flows have simulated wind in urban areas (Britter & Hanna, 2003; Lopez & Garcia, 2001; Sanz, 2003), knowledge of the turbulence generated by VAWTs may help to

improve their performance and efficiency in such areas. One study reported an increased power-collection capability for these turbines in close proximity because they maximize power generation per surface area (Dabiri, 2011). The study of the turbines in close proximity is essential in urban installations of wind turbines due to urban real-estate limitations. In addition, instrumental measurements of the vortices, turbulence and eddies generated by VAWTs are rarely reported (Ferreira, van Bussel, & van Kuik, 2006), as most published works have focused on horizontal axis wind turbines (Ebert & Wood, 1997; Vermeer, Sorensen, & Crespo, 2003; Yang, Sarkar, & Hu, 2012).

In this experiment, turbulence statistics were applied to the upwind and downwind flows of a VAWT. Turbulent statistics are commonly used in the micro-meteorological field. The turbulence generated by a VAWT can be quantified by the fluctuation of the three-directional wind components of the mean wind speed, which are, u' , v' , and w' . Although most VAWTs are positioned at a low hub height, where the atmospheric conditions may not have any influence, taller and larger VAWTs are progressively being developed. Furthermore, a study has shown that the power output of wind turbines can be affected by atmospheric stability, which in turn governs atmospheric turbulence, thus linking the two fields (Wharton & Lundquist, 2012). This paper reports results the turbulence statistics, including variances and spectra, generated by a generic Darrieus-type VAWT.

1.2 Theoretical Framework: Turbulence Statistics

Wind speed fluctuations create turbulence in the mean wind flow. These fluctuations are composed of random wind vectors in three-dimensional space. Steady-state wind flow has a low turbulence intensity, while unsteady-state wind has a high turbulence intensity. Turbulence intensity is a common term used to express the turbulence level.

Coordinates can be superimposed onto these vectors by adding reference axes, namely the orthogonal x - y - z axes. Thus, the wind vectors can be mapped onto the three perpendicular directions of the x - y - z axes, with notations of u , v , and w , respectively, to denote the longitudinal, lateral, and vertical directions.

If flow conditions are statistically stationary with time and Taylor's frozen hypothesis applies for turbulence intensities $I_{u,v,w} = \sigma_{u,v,w}/\bar{u} < 0.5$, where \bar{u} is mean wind speed, turbulence can be quantified by the deviation or standard deviation of the instantaneous wind velocity u' , v' , and w' from the mean wind direction \bar{u} , \bar{v} , and \bar{w} at a single measurement point. The instantaneous wind velocities are u , v , and w .

The standard deviations of the instantaneous velocities u , v , and w are a quantification of the turbulence in the three directions and are usually denoted as σ_u , σ_v , and σ_w . This method of turbulence quantification has been used in the micro-meteorological field since the early 1900s in homogeneous and heterogeneous landscapes (Roth, 2000).

The friction velocity, or u_* , indicates the magnitude of momentum transferred and is also called the shear velocity because wu is (shear stress/density). It can be calculated using Equation (1) where the bars over the letters indicate ensemble averages. This equation can be used in the experimental setup because of the stable nature of the flow generated; the values obtained would be local or unique to a certain measurement position within the flow.

$$u_* = \sqrt{\overline{w'u'^2} + \overline{w'v'^2}} \quad (1)$$

Friction velocity, or u_* , is a usual "scaling" parameter used when creating turbulence vertical profiles of the surface layer of the atmosphere because it is known to be constant with height in the latter layer. In the urban roughness sublayer, the atmospheric layer above the urban or rough surface, its value is lower than the former (Roth, 2000). Reducing the mean wind flow energy is the general method employed to quantify VAWT efficiency. In the context of this experiment, u_* can be used to judge the combined horizontal (u and v) and vertical (w) reductions in kinetic energy downwind of the VAWT.

Turbulence spectral analysis, which is another method used to analyze the instantaneous wind velocity components, reveals important information such as the peak frequency and the rate of decay or generation of spectral power with dimensionless frequency. The method used by Kaimal et al. (1972) has been the standard among micro-meteorologists and was used in the current study for which the ordinate was the non-dimensional spectral power, $nS_{u,v,w}(n)/\sigma_{u,v,w}^2$ or S_p , where $S(n)$ is the spectral power as a function of frequency (Hz), n , and the abscissa is the dimensionless frequency, $f = nL/\bar{u}$, where L is the distance from the wind source. The blade passing frequency (blade rotation frequency) can also be ascertained from the resulting spectra. When flow conditions are statistically stationary, the eddy size can be estimated from S_p and its corresponding turbulence statistics, σ_i , L , and \bar{u} through dimensional analysis. The eddy size in can be written as Equation (2).

$$l_e = \sqrt{S_p \times \sigma_i} \times \frac{L}{\bar{u}} \quad (2)$$

where

$l_{e,i}$ = eddy length, m

$i = u, v$ or w

2. Methodology

2.1 Experimental Set-Up

This experiment was conducted in a laboratory to avoid the influence of external winds and other uncontrollable factors that might affect the readings taken by the sonic anemometer (Young Model 81000). The anemometer is able to measure high frequency wind velocity components of up to 20 Hz. Data logging was conducted by connecting the sonic anemometer to a personal computer (PC). An industrial blower and three industrial fans were used as the wind source, with the height of the middle fan being altered. The VAWT was a Darrieus-type turbine, as shown in Figure 1, and was acquired from iWind Energy (M) Sdn. Bhd. (model no.: iW301). The specifications of the turbine are listed in Table 1. The power, P , versus revolutions per minute, rpm, and the rpm versus \bar{u} of the tested VAWT were provided by manufacturer and are shown in Figures 2 (a) and (b), respectively. As detailed later in this paper, the rpm values ranged from 50–100 rpm, while the apparent wind speed was between 2–3 m/s for Type 1 flow (using blower). For Type 2 flow (using industrial fans), the rpm values ranged from 100–150 rpm, while the range of the apparent wind speed was between 5–6 m/s.

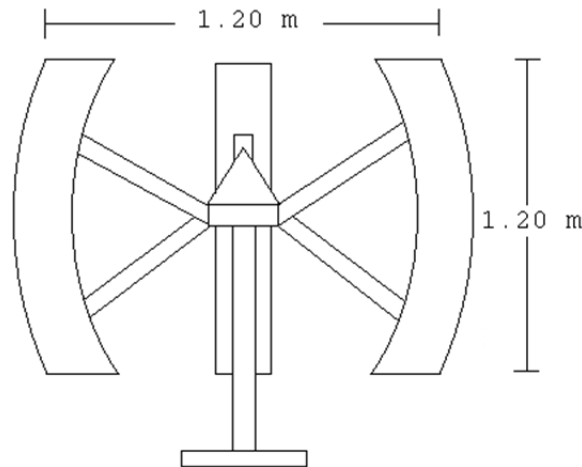


Figure 1. Schematic of the three-bladed Darrieus-type vertical axis wind turbine (VAWT) employed in this experiment

Table 1. Vertical axis wind turbine (VAWT) specifications

Specification	
Rated power output	300 W
Rated wind speed	12 m/s
Cut-in wind speed	2.5 m/s
Survival wind speed	30 m/s
Total swept area	1.44 m ²

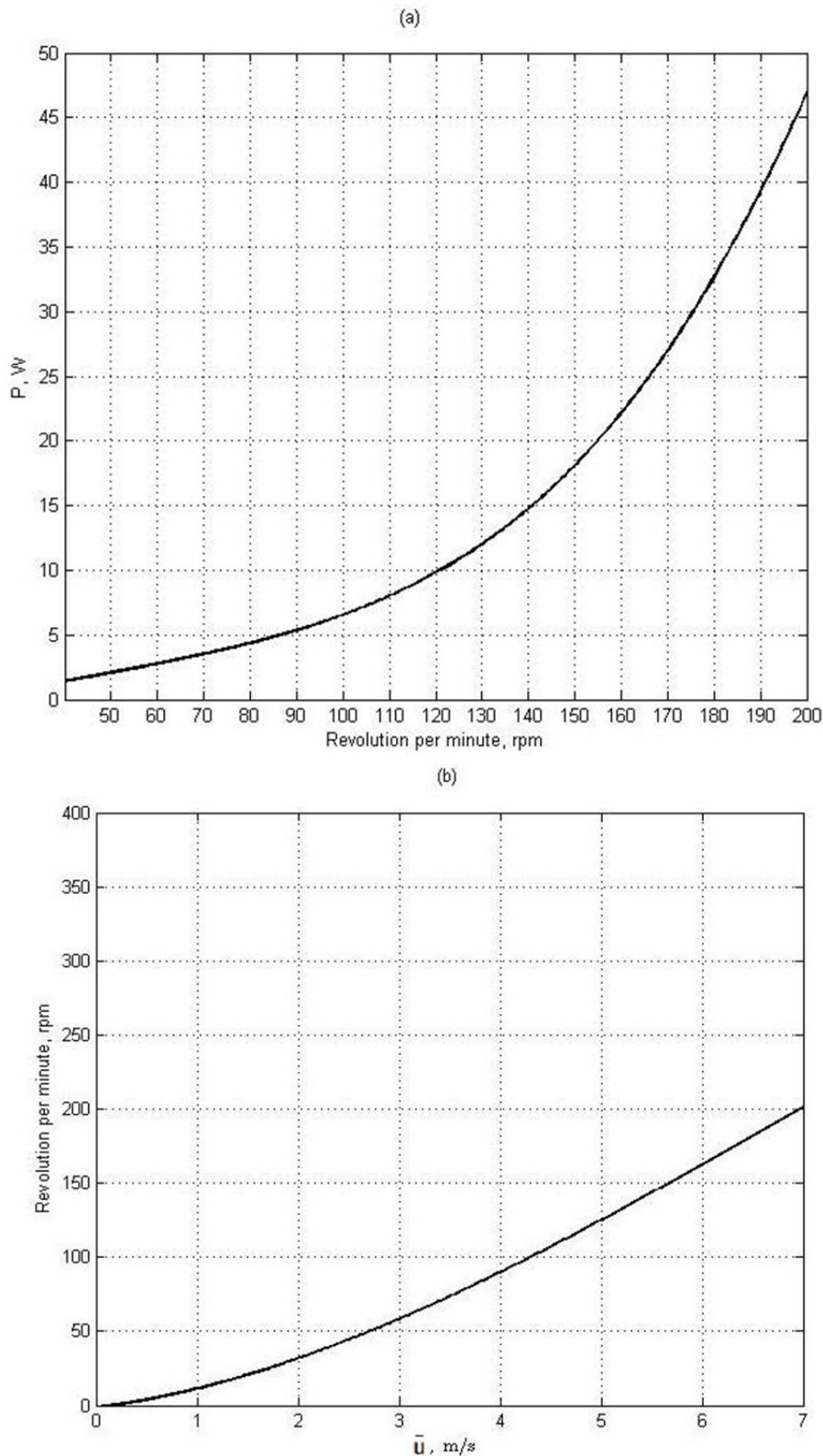


Figure 2. (a) Power, P , versus rpm and (b) rpm versus mean wind speed, \bar{u} , of the tested vertical axis wind turbine (VAWT) as stated by the manufacturer

Throughout the experiment, two types of wind flows were simulated using an industrial blower and industrial fans at three different speeds obtained by adjusting the speed control buttons: low \equiv 1, medium \equiv 2, and high \equiv 3. For Type 1 flow, the blower was aligned with the center of the sonic anemometer (shown in Figure 3). Despite

being very high at the outlet, the speeds were slower downwind. The flow in this case was not uniform, and because this was a pilot study, only the center line of the flow point was considered. For Type 2 flow, three industrial fans were arranged in a row, and the height of the middle fan was lowered (shown in Figure 4). Type 2 flow covered a larger wind source area compared to Type 1 flow. We used three industrial fans in Type 2 flow because we want to maintain a uniform flow condition as the flow disperses downwind. A similar fan configuration, implemented at the indoor testing facility of Universiti Teknologi Malaysia, was used as a reference to this research work (Wahab & Chong, 2003). The turbulence statistics for the flows for different positions at a wind speed of 3, the high setting, are summarized in Table 2. The accuracy of the velocity measurements of the sonic anemometer used is $\pm 1\%$ root mean square, and the mean velocities in the y and z directions were negligible. Different blower speed options from low to high were later discovered to produce the same mean wind speeds. Only the highest speed option was chosen for further analysis. Measurements were taken three times to obtain averages.

The difference between the three ergodic experiments was small, as indicated by the small standard error of the mean wind speed, \bar{u} (refer to Table 2). Although the flow may not have been uniform, this was a preliminary study to explore the turbulence statistics and spectra profiles of a VAWT, which have never been measured before. Furthermore, averaging the flow for 30 min gave stable results (Table 2), suggesting that non-simultaneous measurements before and after the VAWT were not necessary for either type of flow. This experimental setup is similar to that used in a wind tunnel study by Cao et al. (2011) in which the wind velocity ranged from 3–20 m/s with 0.5% turbulence. One benefit of using a blower is that the turbulent component frequency and energy at the nozzle should be similar, unlike natural wind. Meanwhile, the positioning of the three industrial fans for Type 2 flow covered a larger wind source area.

Table 2. Summary of the turbulence standard deviations and friction velocities (at 30-min averages) for positions A, B, C, and D at speed 3 (high setting) for Type 1 and Type 2 flow; note that all parameters of A and C have similar values even though measurements were non-simultaneous for Type 1 flow; the results are reported as the mean \pm standard error, where standard error = $\sigma/n^{1/2}$ where σ = standard deviation and n = number of data points

Position (Type of flow)	L (m)	\bar{u} (m/s)	σ_u (m/s)	σ_v (m/s)	σ_w (m/s)	u^* (m/s)
A (T1)	0.5	12.6 \pm 0.2	0.613 \pm 0.004	0.432 \pm 0.002	0.378 \pm 0.007	0.281 \pm 0.014
B (T1)	2.0	5.04 \pm 0.04	1.24 \pm 0.01	0.724 \pm 0.004	0.763 \pm 0.001	0.305 \pm 0.008
C (T1)	0.5	13.0 \pm 0.1	0.602 \pm 0.004	0.422 \pm 0.005	0.376 \pm 0.000	0.259 \pm 0.003
D (T1)	2.0	3.84 \pm 0.04	1.05 \pm 0.02	1.77 \pm 0.02	0.672 \pm 0.024	0.656 \pm 0.016
A (T2)	0.5	6.41 \pm 0.018	2.387 \pm 0.048	0.722 \pm 0.005	0.573 \pm 0.004	0.387 \pm 0.006
B (T2)	2.0	3.72 \pm 0.019	1.237 \pm 0.003	0.620 \pm 0.001	0.611 \pm 0.003	0.359 \pm 0.001
C (T2)	0.5	6.21 \pm 0.043	1.210 \pm 0.040	0.486 \pm 0.001	0.484 \pm 0.007	0.555 \pm 0.012
D (T2)	2.0	0.46 \pm 0.002	0.363 \pm 0.003	0.202 \pm 0.002	0.230 \pm 0.003	0.059 \pm 0.004

The results are reported as the mean \pm standard error, where standard error = $\sigma/n^{1/2}$ where σ = standard deviation and n = number of data points. T1 indicates Type 1 flow (using a blower), and T2 indicates Type 2 flow (using industrial fans).

Two measurement positions from the blower (Type 1 flow) and industrial fans (Type 2 flow) and two configurations with and without the VAWT were chosen: position A ($L = 0.5$ m), B ($L = 2.0$ m), C ($L = 0.5$ m) and D ($L = 2.0$ m downwind) (refer to Figure 3 and Figure 4). For positions A and B, the turbulence data were collected without the VAWT to serve as experimental controls, while for positions C and D, the VAWT was installed. The voltage, V , was recorded every 15 min with the VAWT.

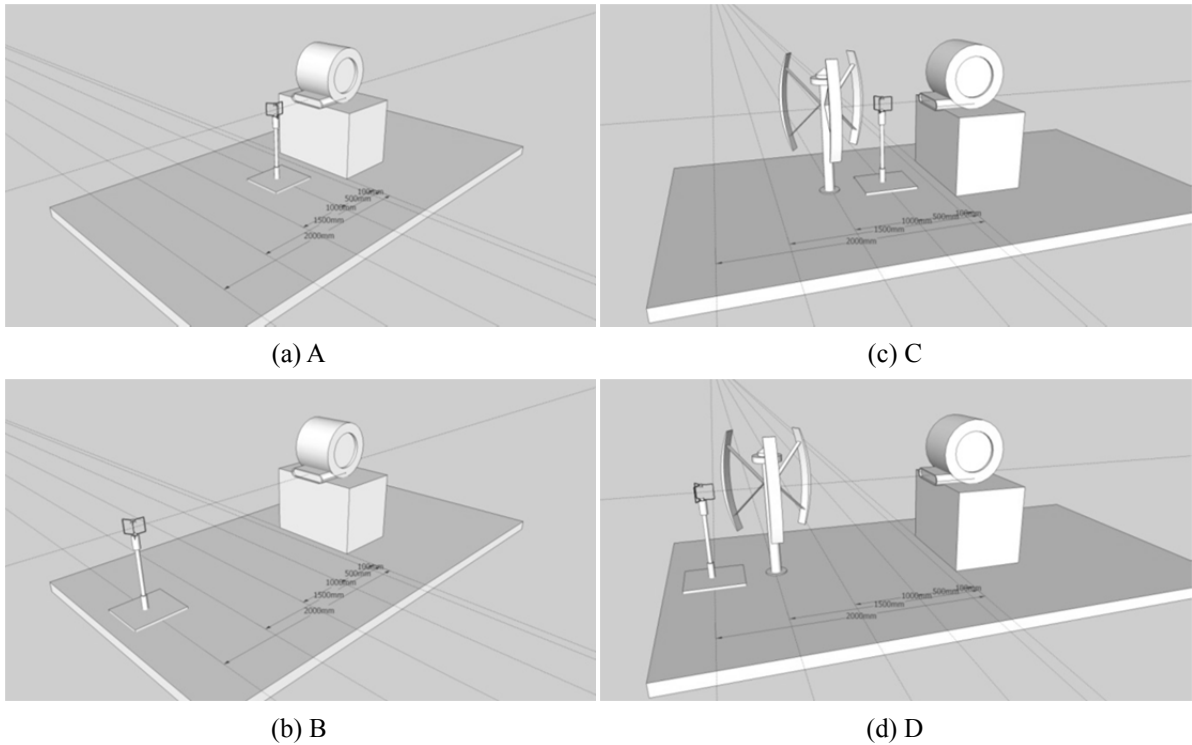


Figure 3. Experimental setup depicting the vertical axis wind turbine (VAWT), blower, and sonic anemometer for Type 1 flow at positions A, B, C and D; runs for positions A and B were without the VAWT, while positions C and D included the VAWT

The sonic anemometer was connected directly to a PC using a RS232 cable and the “Hyperterm” computer program as an interface. Wind component velocities were recorded at a sample rate of 10 Hz (0.1 s). During the experiment, a radius of 0.5 m around the blower, industrial fans, sonic anemometer, and VAWT was cleared to avoid any wind flow obstructions or wakes. An averaging time of 30 min was used to compute the turbulence statistics. As discussed later, this is a reasonable averaging time to use in this situation because it creates a statistically stationary condition for the momentum fluxes. This averaging time has also been used in micro-meteorological studies of urban areas (Yusup, 2012).

For the entire experiment, the angular velocity of the turbine was 5.2–6.3 rad/s or 50–60 rpm for Type 1 flow and 7.3–15.7 rad/s or 70–150 rpm for Type 2 flow, as determined from the display panel of the VAWT. The angular velocity, ω , can be calculated from Equation (3).

$$\omega = 2\pi f \quad (3)$$

where

ω = angular velocity (rad/s)

f = rotational frequency (Hz or s^{-1})

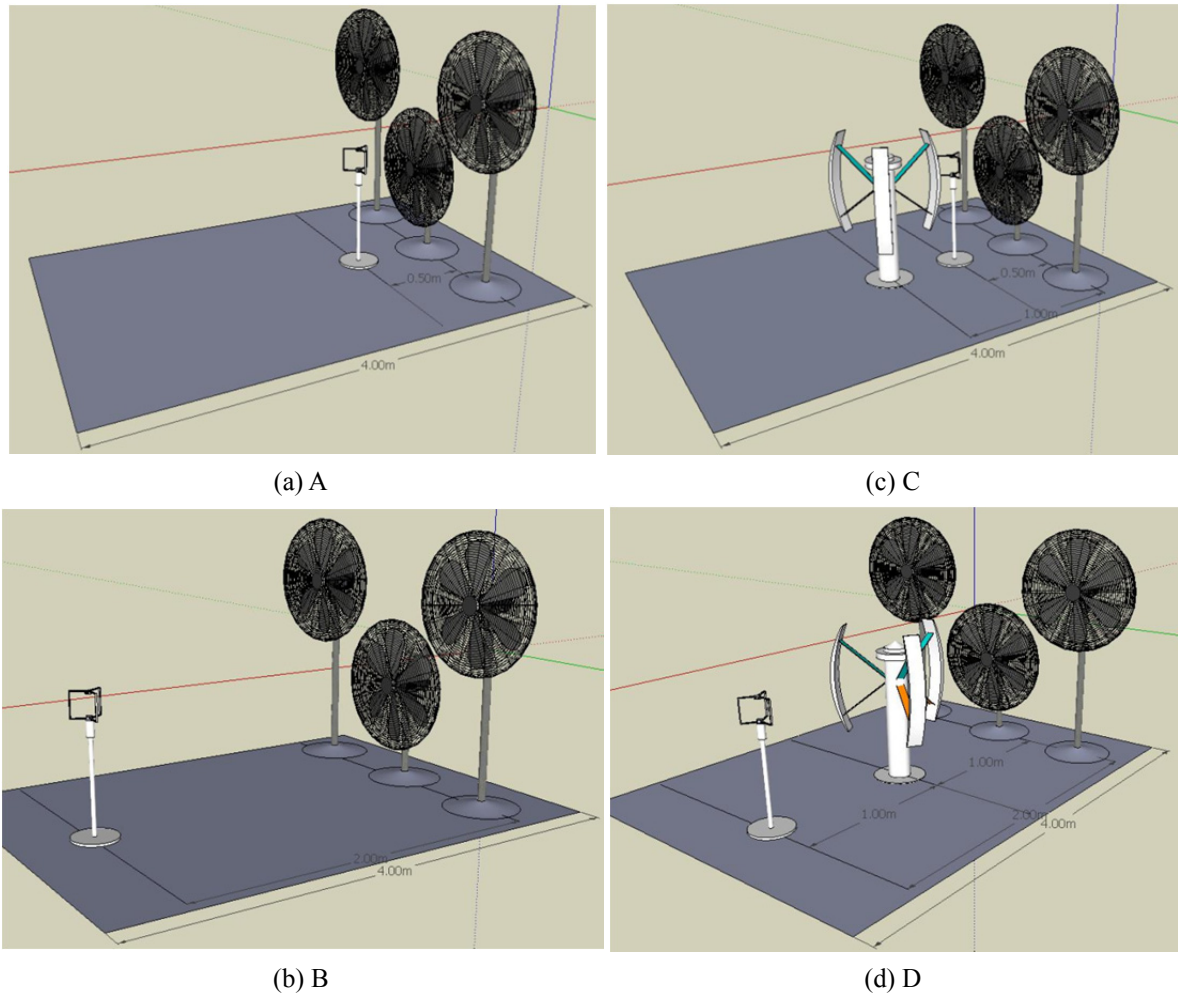


Figure 4. Experimental setup depicting the vertical axis wind turbine (VAWT), industrial fans, and sonic anemometer for Type 2 flow at positions A, B, C and D; runs for positions A and B were without the VAWT, while positions C and D included the VAWT

From the power, rpm, and wind velocity curves given by the manufacturer, the apparent wind velocity was determined to be 3–4 m/s (from Figure 2 (b)), which was different from the range of 11–12 m/s measured by the sonic anemometer before the VAWT (positions A and C), indicating that only a fourth of the wind speeds were harnessed by the VAWT. As detailed in this paper, the rpm range for Type 1 flow was between 50–100 rpm, and the apparent wind speed was between 2–3 m/s. For Type 2 flow, the rpm range was between 100–150 rpm, and the apparent wind speed was between 5–6 m/s. These results were further corroborated by the amount of P generated, which was within the range of 1–3 W for Type 1 flow and 7–15 W for Type 2 flow (see Figure 2 (a)). From these values, the estimated tip speed ratio (TSR), λ , for mean wind speeds of 3 m/s for Type 1 flow and 5 m/s for Type 2 flow was calculated using Equation (4) to be 1.0–1.2 and 0.9–1.9.

$$\lambda = \frac{\omega r}{\bar{u}} \quad (4)$$

where

r = rotor radius = 0.6 m

\bar{u} = mean wind speed

The TSR of a wind turbine depends on the number of blades; the optimal TSR values of two-bladed, three-bladed, and four-bladed rotors are 6.28, 4.19, and 3.14, respectively (M. Ragheb & A. M. Ragheb, 2011). The optimal λ for a three-bladed wind turbine is well above the λ_{op} found in this experiment.

The power coefficient, C_p , of a VAWT can be calculated using Equation (5). The C_p calculated for both flows was approximately 9% based on mean wind speeds of 3 m/s for Type 1 flow and 5 m/s for Type 2 flow. The

extractable power was 2 W for Type 1 flow and 10 W for Type 2 flow.

$$C_p = \frac{P}{W} = \frac{P}{\frac{1}{2} \cdot \rho \cdot S \cdot \bar{u}^3} \quad (5)$$

where

P = power, W

W = kinetic power

ρ = density of air $\approx 1.2 \text{ kg/m}^3$

S = swept area for turbine = 1.44 m^2

2.2 Data Analysis

In this work, high-frequency three-dimensional wind speed measurements (u , v , and w) were collected. Data were processed using Matlab 2008b (MathWorks, USA). Data processing includes data filtration, turbulence statistics calculations, and spectral analysis. Data quality checks and filtration (such as data spikes removal) were also performed. The standard deviations of the fluctuations of u , v , and w from the mean, i.e., σ_u , σ_v , and σ_w , were then calculated. The Fast Fourier Transform or FFT function in Matlab was used for spectral analysis. FFT converts time series signals (or data) by changing the time domain to the frequency domain and the magnitude domain to the spectral power domain. The plot of the spectral power versus frequency would reveal the signal's periodic pattern, i.e., distribution of energy at different frequencies.

2.3 Scope and Limitations of Study

Wind speeds produced by the industrial blower were not uniform. Since this is a pilot study, only the center line of the flow is considered. The amount of turbulence generated at the entrance of the experimentally observed section was not controlled, i.e., the upwind area before the VAWT.

3. Results and Discussion

3.1 Standard Deviations of the Wind Component Fluctuations for the Darrieus VAWT

The turbulence statistics are summarized in Table 2. The values shown are averaged. The turbulence statistics σ_u , σ_v , and σ_w were similar for repeated experiments, with low standard deviations in the range of 0.001–0.010 for the three wind speeds. These statistics did have a relatively higher variation on the order of 0.02 for the standard errors for position D (Type 1 flow with the VAWT) compared to the other positions. This variation was expected because these turbulence statistics should include the turbulence generated by the VAWT. The turbulence intensities, I , were also found to be < 0.5 for this dataset, validating Taylor's frozen hypothesis and the use of a 30 min averaging time. If fans are used as a wind source, an averaging time of greater than 90 min is required to stabilize the turbulence spectra at lower dimensionless frequencies, $f < 0.01$.

For brevity, only the summarized results for the speed \equiv value of 3 (high) are listed. These values show consistent trends with the two lower speed settings. Type 1 flow had a higher mean wind speed (\bar{u}) and lower turbulence standard deviations (σ_u , σ_v , σ_w) than Type 2 flow for Position A; while for Position B, the \bar{u} was lower for Type 2 flow compared to Type 1 flow, although the σ_u , σ_v and σ_w were mostly the same. The friction velocities had the same magnitude for both types of flow. For Type 1 flow, the mean wind speed, \bar{u} , decreased by 60% from 12.6 m/s to 5.04 m/s from position A to position B downwind of the blower for runs without the VAWT. Conversely, for runs with the VAWT (positions C and D), there was a 70% reduction in wind speed from 13.0 m/s to 3.84 m/s. The turbulence parameters increased with distance, L and \bar{u} . There was a 51% increase in σ_u from 0.613 m/s to 1.24 m/s without the VAWT, but only 43% increase from 0.602 m/s to 1.05 m/s when the VAWT was used. As for σ_v , a 41% increase from 0.432 m/s to 0.724 m/s was observed without the VAWT, while a 76% increase from 0.422 m/s to 1.77 m/s was observed with the VAWT. For σ_w , a 50% increase from 0.378 m/s to 0.763 m/s was observed without the VAWT, while a 44% increase from 0.376 m/s to 0.672 m/s was observed with the VAWT. For Type 2 flow using industrial fans and without the VAWT, \bar{u} decreased from 6.41 m/s at position A to 3.72 m/s at position B, for a total decrease of 42%. With the VAWT installed, \bar{u} fell by 90% from 6.21 m/s at position C to 0.46 m/s at position D. Turbulence decreased with distance by 48% from 2.387 m/s at position A to 1.237 m/s at position B without the VAWT, while it decreased by 70% from 1.21 m/s at position C to 0.363 m/s at position D with the VAWT. The parameter u^* , which is proportional to wind speed (Yusup, 2012), increased by 40 to 55% with the VAWT and by $< 10\%$ without the VAWT, indicating the transfer of a significant amount of vertical momentum when wind flows through the turbines. This result agrees with the findings of Dabiri (2011) that show VAWTs' ability to extract planform (from the top) kinetic energy.

The highest increase of the three turbulence statistics was found in σ_v for Type 1 flow when the VAWT was used.

A relative decrease in σ_u and σ_w was observed for Type 1 flow; and σ_u , σ_v and σ_w decreased for Type 2 flow when the VAWT was within the flow. The 40% increase in u^* was caused by heightened lateral wind fluctuations, v' , of the spinning VAWT.

3.2 Spectral Characteristics of the Wind Components

Using FFT, we obtained spectral power and frequency. These plots showed the distribution of spectral power at different frequencies also revealing energy peaks and dips at discrete frequencies. A plot of the magnitude of a time-series input signal versus dimensionless frequency could be used to reveal the signal's periodic pattern. Figure 5 shows the spectral power for both upwind and downwind flows before normalization. Dissipation still occurred from upwind positions such as A and C, to downwind positions, such as B and D, at higher frequencies. The spectral power decreased with distance due to the lower wind component fluctuations (turbulence intensity) associated with the lower mean wind speeds downwind. We could not compare the upwind and downwind u , v , and w spectra without normalizing them with σ_i^2 .

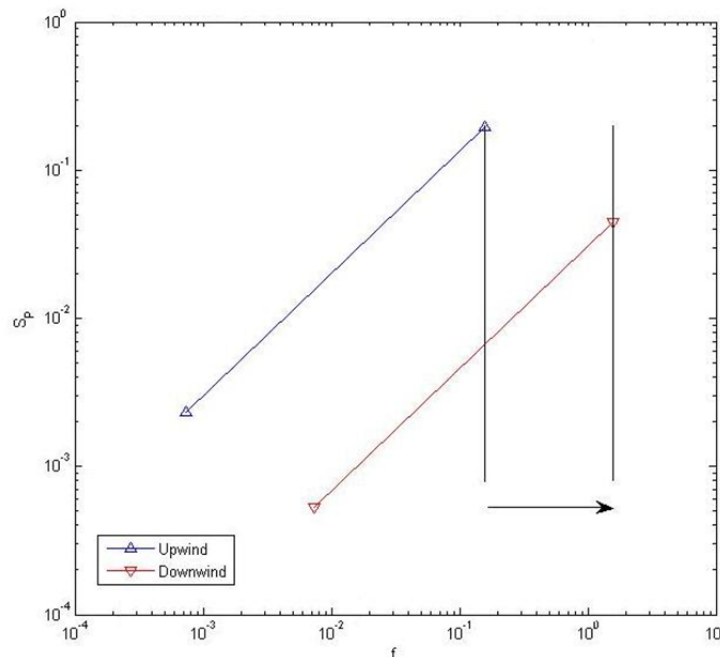


Figure 5. Schematic of the spectral power for both upwind and downwind flows before normalization; energy dissipation occurred from upwind to downwind or was displaced to higher frequencies (to the right)

The three speeds for Type 1 flow (low, 1: $\bar{u} = 11.7$ m/s; medium, 2: $\bar{u} = 12.1$ m/s; and high, 3: $\bar{u} = 12.6$ m/s) did not exhibit much difference in terms of normalized spectral power, S_p , and f thus only speed 3 is displayed and discussed because the other speeds showed similar trends and magnitudes. The normalized dimensionless frequency, f , ranged from 0.00001 to 10. The plot in Figure 6 shows the upwind and downwind (without VAWT) spectra for Type 1 and Type 2 flows, which are separated by a factor of ten (one period) for the dimensionless frequency, f , parameter. The resulting spectra trend of Type 1 flow is similar to that of Type 2 flow, although the wind mean speeds were higher and the three wind vector fluctuation standard deviations (σ_u , σ_v , and σ_w) were lower for the Type 1 flow. Figure 6 exhibits higher dimensionless frequency ranges for the downwind flow compared to the upwind flow, although both show a similar increasing trend with dimensionless frequency. The dissipation occurred at higher frequencies with distance from wind source, similar to other flow types such as atmospheric wind, and at to lower frequencies for the same distance category (downwind or upwind) from the wind sources (blower or industrial fans). For Type 2 flow, the spectral power was constant, or the eddy size was constant, at a high dimensionless frequency range from 0.007 to 0.04. This might be due to the fan configuration, which covered a larger wind-swept area.

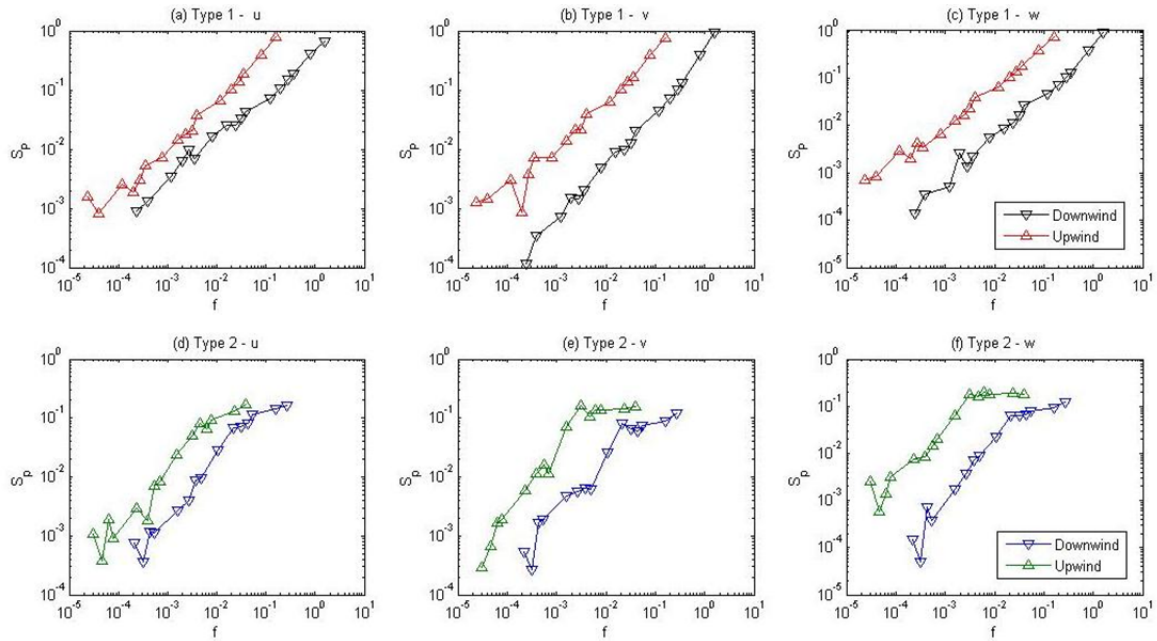


Figure 6. Upwind and downwind spectral power (normalized) of components u , v , and w , for Type 1 and Type 2 flows without the VAWT for positions A and B; only “high” or speed 3 shown here; a similar trend can be seen for both upwind and downwind flows, although because the flow were offset by a factor of ten, the axis of f (dimensionless frequency, where $f = nL/\bar{u}$. Frequency (Hz), n , was normalized by distance/mean wind speed, L/\bar{u} , to facilitate comparison

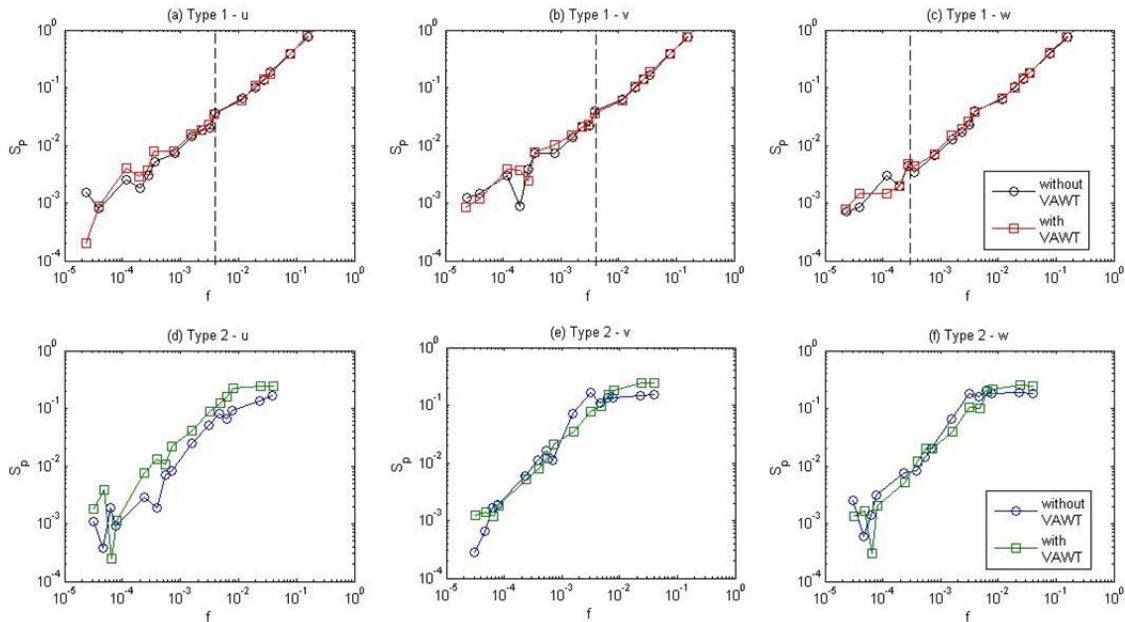


Figure 7. Upwind spectral power (normalized) of components u , v , and w , for Type 1 and Type 2 flows, with and without the VAWT, for positions A and C; only “high” or speed 3 shown here, which exhibited a spectral trend not affected by the presence of the VAWT upwind; the vertical dash lines for (a) and (b) are for $f = 0.004$ and for (c) $f = 0.0003$ (where $f = nL/\bar{u}$), indicating the influence of surrounding obstacles for Type 1 flow; the frequency (Hz), n , was normalized by distance/mean wind speed, L/\bar{u} to facilitate comparison

The spectra of u , v , and w , with and without the VAWT, are shown in Figure 7 for positions A and C at 0.5 m downwind from the blower and industrial fans. Low dimensionless frequency values of S_p were scattered; $f < 0.004$ for u and v , while $f < 0.0003$ for w for Type 1 flow. These ranges indicate external influences on S_p in the

latter low dimensionless frequency ranges originating from the surrounding area. The influences could have been wakes formed by obstacles or the blower itself. The components u and v should be more affected by these influences than w , just as they would be for atmospheric wind flow on rough surfaces such as urban morphologies (Yusup, Daud, Zaharim, & Talib, 2008). Figure 7 shows a similar pattern when the VAWT was not within the flow (position A) and when it was within the flow (position C), implying that the spectral characteristics of the upwind flows were unaffected by the VAWT. As mentioned earlier, because Type 2 flow had a larger wind-swept area, the spectral power was approximately constant at high dimensionless frequency values of $0.007 < f < 0.04$.

The observations for position B were controls for the observations for position D (flow after the VAWT). The spectra of position D shown in Figure 8 exhibit interesting features, such as the dip and peak of S_p for Type 1 flow at the dimensionless frequencies and power listed in Table 3. For Type 1 flow, the dip and peak of S_p decreases with the decreasing dimensionless frequency in distinct dimensionless frequency ranges of $0.003 < f < 0.02$ for u and v . As for w , the dimensionless frequency range is in a narrower band, $0.003 < f < 0.005$. The maximum magnitude of S_p for u and v after the dip is on the order of 5 times and 17 times w , respectively. In Figure 8, with the VAWT, and at a normalized dimensionless frequency, $f = 1$, there is a small peak, which is obvious for v , corresponding to the blade passing frequency of 45 rpm. For Type 2 flow, dips only appear at dimensionless frequencies of 0.0025 for u and 0.0035 for v and w . Every 10.7 min and at 0.00156 Hz, Type 1 flow with the VAWT produced a peak in spectral power, while every 1.5 min and at 0.0109 Hz, Type 2 flow with the VAWT produced a dip in spectral power. Hence, the VAWT with Type 2 flow absorbed more kinetic energy than Type 1 flow due to the larger swept area of the Type 2 flow.

Table 3. Maximum and minimum normalized spectral power, S_p , and normalized frequency, f , of u , v , and w of Type 1 and Type 2 flow at position D for speed 3 (high setting)

Type of flow	\bar{u} (m/s)	Wind component	Maximum (peak)		Minimum (dip)	
			f	S_p	f	S_p
1	3.84	u	0.003	0.1	0.02	0.007
		v	0.003	0.02	0.02	0.002
		w	0.003	0.006	0.005	0.003
2	0.46	u	-	-	0.0025	0.0006
		v	-	-	0.0035	0.00006
		w	-	-	0.0035	0.00025

- data not available.

Based on the S_p values of Figure 6 for positions A and B, the turbulent eddies of u , v , and w dissipated in the low dimensionless frequency ranges at the same distance from the wind source but shifted to the right from upwind position A to downwind position B, indicating dissipation in the high dimensionless frequency range with distance from the wind source. The rates of dissipation at positions A and C with the VAWT were similar for u , v , and w (refer to Figure 7). Referring to Figure 8, the rates of dissipation at position D for the u and v components were in the high dimensionless frequency range (dip) compared to w for Type 1 flow. Meanwhile, the dips observed in Type 2 flow were almost at the same dimensionless frequency range for u , v and w .

The high spectral power at the high dimensionless frequencies observed in the spectra can be explained by the nature of the source: an industrial blower. This blower consists of small spinning rotors that generate high energy eddies at high dimensionless frequencies, as reflected in the spectra given here. As the wind moves downwind, the eddies dissipate and concurrently decrease in size and frequency. The spectral trend and magnitude scatter should be at a minimum because they originate from the same source. Any scatter observed in this experiment could have been caused by external influences that primarily affected the spectral power at lower frequencies, $f < 0.004$ for u and v and $f < 0.0003$ for w (refer to Figure 7), when the industrial blower was used in Type 1 flow. We observed more scatter in the spectral trend for Type 2 flow at lower dimensionless frequencies ($f < 0.0006$) compared to that of Type 1 flow. Considering the low dimensionless frequency “noise”, the results show that the VAWT was able to reduce the horizontal turbulent component energies (u and v) in a dimensionless frequency

range of 0.003–1. The VAWT introduced general dominant eddy-normalized frequencies of dips and peaks independent of the mean wind speed. These center line eddies of flow had low dimensionless frequencies ($f \approx 0.002$) and were large in size at $L = 2$ m and $\bar{u} = 3.84$ m/s for Type 1 flow at position D: 17 cm for u , 10 cm for v , and 3 cm for w . When the air left the blower’s nozzle, the dimensions of u , v , and w were 0.4 cm for Type 1 flow at position C. The eddies in Type 2 flow were smaller compared to those in Type 1 flow; u was 6.4 cm at $f = 0.0025$, and v and w were 1.5 cm and 3.3 cm, respectively at $f = 0.0035$.

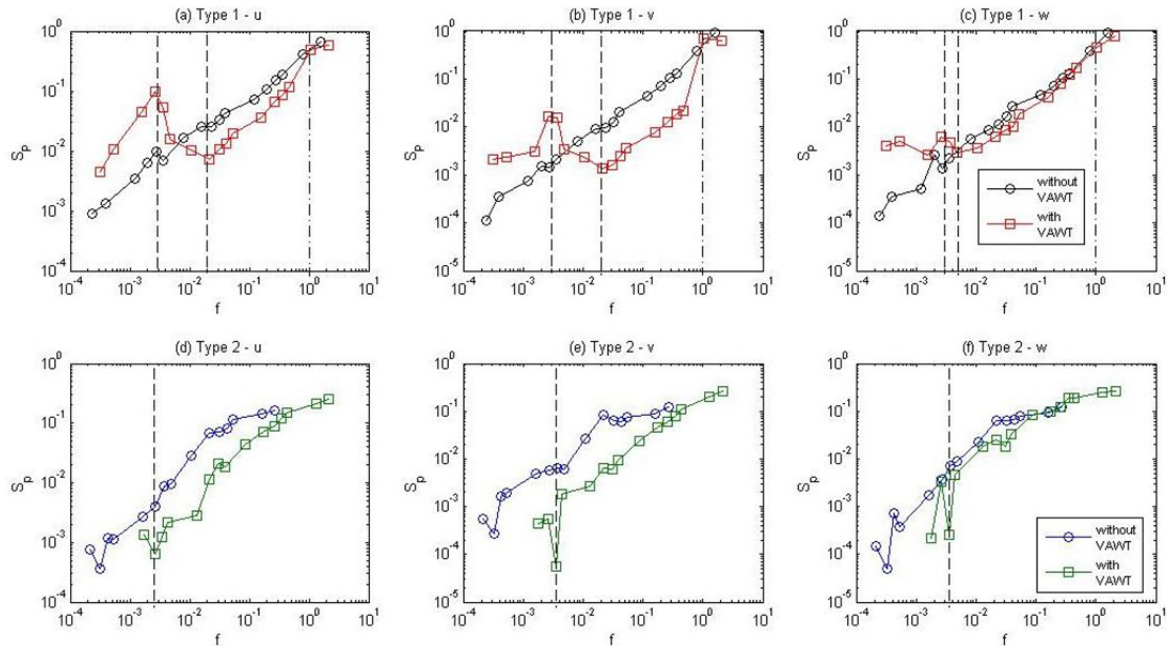


Figure 8. Downwind spectral power (normalized) of components u , v and w for Type 1 and Type 2 flows with and without the VAWT for positions B and D; only “high” or speed 3 shown here; these plots show the dip and peak frequencies induced by the VAWT at dimensionless frequencies marked by the vertical dashed lines; the dashed dot bolded lines show the blade passing frequency; frequency (Hz), n , was normalized by distance/mean wind speed, L/\bar{u} , to facilitate comparison

Various eddy sizes at different f values are listed in Table 4, which lists the original size of the eddy at the blower’s nozzle, the size upwind of the industrial fans (position C), and the size at the dip and peak frequencies after the VAWT (position D). For the normalized spectra, the high values of σ_v presented in Table 2 cannot be seen here because the values were normalized to compare the distinct features of the spectral characteristics. Figure 9 shows that component v had the highest turbulence intensity, followed by u and w , after removing normalizing factors. Components u and v exhibited similar spectral trends with a distinct set of large eddies at $f = 0.0015$ Hz and small eddies at $f = 0.01$ Hz for u and v . These results reveal a long period pattern within the flow after the VAWT that included large and small eddies by a factor of 10 on the frequency scale.

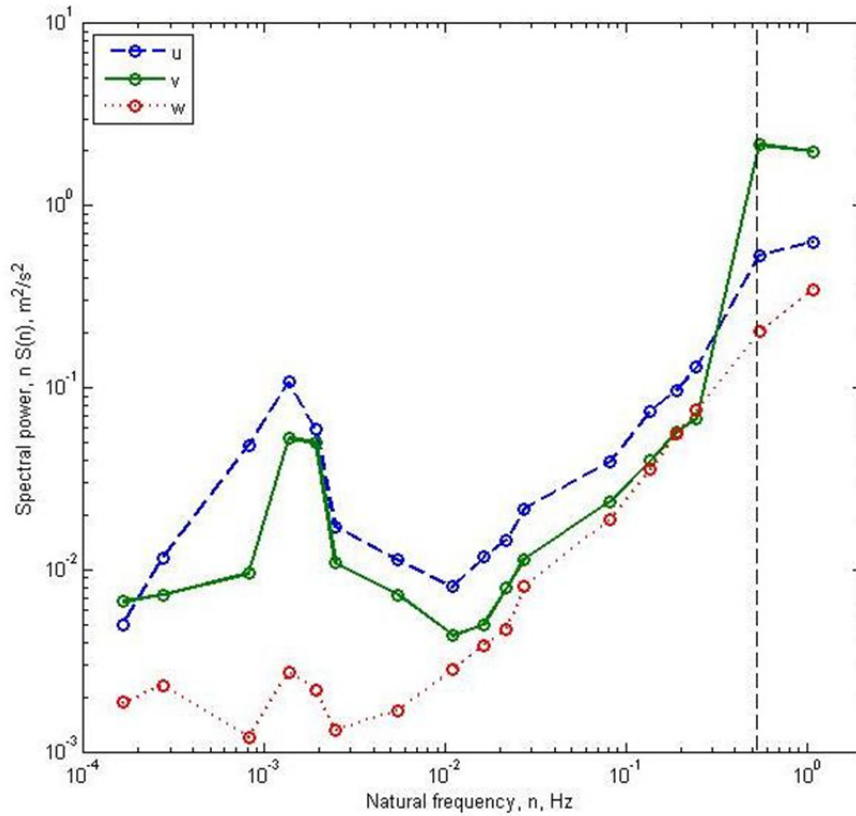


Figure 9. Downwind spectral power of u , v , and w for Type 1 flow, with the VAWT (position D); only “high” or speed 3 shown here; these plots show the dip and peak frequencies induced by the VAWT; the vertical dashed line shows the blade passing a frequency of 0.55 Hz; component v has more turbulence in the high frequency range ($n > 0.4$ Hz) followed by u and w

Table 4. Eddy sizes of wind components u , v , and w for positions C and D with the VAWT and dimensionless frequencies of dips and peaks for Type 1 and Type 2 flows at speed 3 (high setting); at position D, there is an increase in eddy sizes for u , v , and w from dips to peaks for Type 1; position C is listed to show a comparison between the eddy sizes for upwind and downwind flows; note that there are only dips and no peaks at Position D for Type 2 flow

Position (m)	Type of flow	f	Features	$l_{e,u}$ (cm)	$l_{e,v}$ (cm)	$l_{e,w}$ (cm)
C (0.5)	1	0.02	none	1	0.8	0.7
		0.005	none	0.4	0.5	0.5
		0.003	none	0.4	0.4	0.4
D (2.0)	1	0.02	dip (for u and v)	5	3	-
		0.005	dip (for w)	-	-	2
		0.003	peak (for u,v,w)	17	10	3
C (0.5)	2	0.0025	none	2.3	1.3	1.5
		0.0035	none	2.6	1.6	1.8
D (2.0)	2	0.0025	dip (for u)	6.4	-	-
		0.0035	dip (for v,w)	-	1.5	3.3

- data not available.

3.3 Voltage Produced and Turbulence Statistics

In this section, data on the voltage, V , generated at position C is presented. The voltage was proportional only to the rpm of the turbine and not to power production. We observed a positive correlation between \bar{u} and V at position C (refer to Table 5 and Figure 10). A higher wind speed resulted in a higher V ; with every increment in \bar{u} , the voltage increased by 0.5, in agreement with the function of $V = f(\bar{u})$. The relationship between σ_u and V was independent in this study because no significant trend was observed. σ_u was not correlated with V , and the type of flow (Type 1 and Type 2) did not affect σ_u .

Table 5. Voltage (V), rpm (rotation per minute), and turbulence statistics, $\sigma_{u,v,w}$, for Type 1 and Type 2 flows at positions C (upwind) and D (downwind) with the VAWT for all speed settings, 1–3 (low to high)

Position	Speed	V (V)	rpm range	\bar{u} (m/s)	σ_u (m/s)	σ_v (m/s)	σ_w (m/s)
C (T1)	1	3.4		11.8	0.575	0.399	0.361
	2	4.7	-	12.6	0.598	0.418	0.373
	3	5.9		13.0	0.602	0.422	0.376
D (T1)	1	3.4		3.69	1.08	1.70	0.67
	2	4.7	-	3.55	1.07	1.66	0.74
	3	5.9		3.77	0.90	1.74	0.72
C (T2)	1	5	74–80	2.58	1.45	0.525	0.519
	1	5	74–80	2.63	1.54	0.516	0.522
	1	5	74–80	2.59	1.51	0.527	0.515
	2	7	100–105	3.00	1.59	0.616	0.625
	2	7	100–105	3.02	1.62	0.608	0.627
	3	12	148–154	6.13	1.26	0.486	0.492
	3	12	148–154	6.28	1.13	0.484	0.470
	3	12	148–154	6.21	1.24	0.488	0.491
D (T2)	1	5	74–80	0.428	0.312	0.200	0.196
	1	5	74–80	0.421	0.316	0.196	0.197
	2	7	100–105	0.467	0.388	0.218	0.247
	2	7	100–105	0.474	0.388	0.220	0.246
	3	12	160–163	0.46	0.357	0.204	0.224
	3	12	160–163	0.46	0.359	0.206	0.230
	3	12	160–163	0.46	0.366	0.200	0.228

T1 indicates Type 1 flow (using blower) while T2 indicates Type 2 flow (using industrial fans).

- data not available.

4. Future Work

Because this was a pilot assessment of the turbulence generated by a VAWT using turbulence statistics, further experiments should be conducted in a more controlled environment, such as a wind tunnel, so that the wind speeds are uniform and the turbulence manageable. Furthermore, the apparent speeds should be tested at a higher magnitude than what was done in this study, although this will require a larger wind-swept area. Natural wind

should be simulated in the wind tunnel; a peak normalized dimensionless frequency of approximately 1 with turbulence cascading into the higher and lower dimensionless frequencies would give a more realistic scenario of a VAWT operating in the field. In future work, the integral length scale should be studied instead of the eddy size. Multiple sonic anemometers should be installed in three dimensions downwind and upwind of the VAWT at uniform distances to generate a turbulence profile of the wind and its subsequent exhaust following the VAWT.

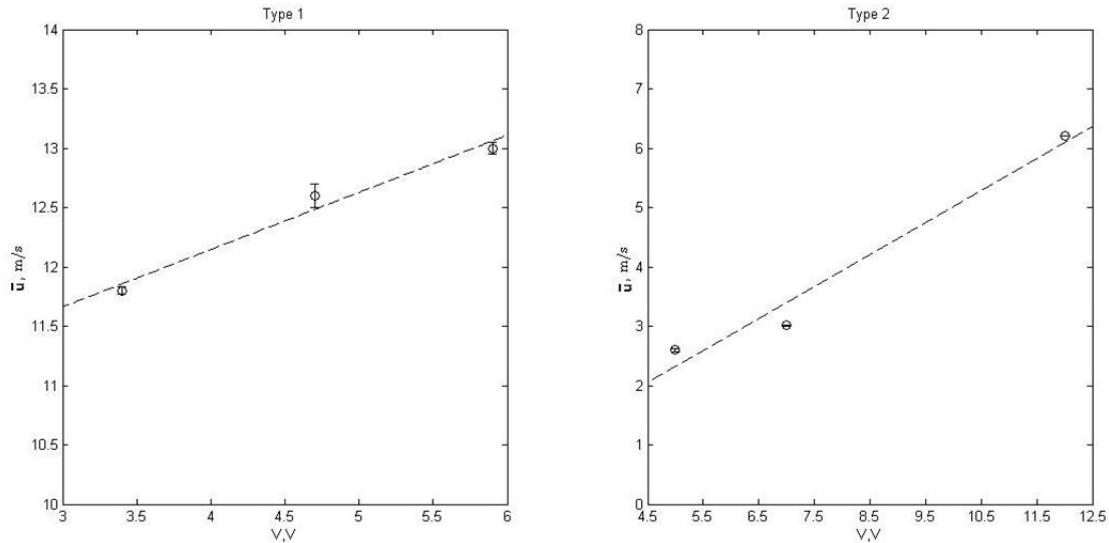


Figure 10. \bar{u} versus Voltage, V for Type 1 and Type 2 flow at position C; dashed lines are best-fit linear regression lines; the slope for both Type 1 and Type 2 flows are approximately the same and equal to 0.5

5. Conclusions

The lateral turbulence, σ_v , in the flow increased downwind of the Darrieus-type VAWT compared to its longitudinal, σ_u , and vertical, σ_w , counterparts. The VAWT was able to reduce the horizontal turbulence component energies (u and v) in a dimensionless frequency range of 0.003–1 and produce two distinct sets of eddies sizes for Type 1 flow: large and small at $f = 0.003$ and $f = 0.02$, respectively. For Type 1 flow, the eddy sizes were large at $L = 2$ m and $\bar{u} = 3.84$ m/s: 17 cm for u , 10 cm for v , and 3 cm for w compared to an initial size at the source of 0.4 cm for all three components. For Type 2 flow, the eddy sizes for u , v and w were smaller at 6.4 cm (at $f = 0.0025$), 2.5 cm and 3.3 cm (at $f = 0.0035$). No peak at position D was observed for Type 2 flow. The VAWT introduced general dominant eddy-normalized dimensionless frequencies of dips and peaks independent of the mean wind speed. A long period pattern was also discovered within the flow after the VAWT that featured large and small eddies differing by a factor of 10 in the frequency scale. Finally, higher wind speeds resulted in higher V generated at a rate of 0.5. No significant trend was observed for the relationship between σ_u and V , but the type of flow did affect σ_u .

Acknowledgements

The research described in this paper was financially supported by the Malaysian Higher Education Institute's Fundamental Research Grant Scheme (FRGS) (grant no.: 203/PTEKIND/6711329) and the Universiti Sains Malaysia (USM) via a short-term grant (grant no.: 304/PTEKIND/6312099).

References

- Britter, R. E., & Hanna, S. R. (2003). Flow and dispersion in urban areas. *Annual Review of Fluid Mechanics*, 35, 469-496. <http://dx.doi.org/10.1146/annurev.fluid.35.101101.161147>
- Cao, N., Ting, D., & Carriveau, R. (2011). The performance of a high-lift airfoil in turbulent wind. *Wind Engineering*, 35(2), 179-196.
- Christen, A., Rotach, M. W., & Vogt, R. (2009). The budget of turbulent kinetic energy in the urban roughness sublayer. *Boundary-Layer Meteorology*, 131(2), 193-222. <http://dx.doi.org/10.1007/s10546-009-9359-5>
- Dabiri, J. O. (2011). Potential order-of-magnitude enhancement of wind farm power density via counter-rotating vertical-axis wind turbine arrays. *Journal of Renewable and Sustainable Energy*, 3(4), 043104. <http://dx.doi.org/10.1063/1.3608170>

- Ebert, P. R., & Wood, D. H. (1997). The near wake of a model horizontal-axis wind turbine—I. Experimental arrangements and initial results. *Renewable Energy*, 12(3), 225-243. [http://dx.doi.org/10.1016/S0960-1481\(97\)00046-3](http://dx.doi.org/10.1016/S0960-1481(97)00046-3)
- Eriksson, S., Bernhoff, H., & Leijon, M. (2008). Evaluation of different turbine concepts for wind power. *Renewable and Sustainable Energy Reviews*, 12(5), 1419-1434. <http://dx.doi.org/10.1016/j.rser.2006.05.017>
- Ferreira, C. J. S., van Bussel, G. J. W., & van Kuik, G. A. M. (2006). Wind tunnel hotwire measurements, flow visualization and thrust measurement of a VAWT in skew. *Journal of Solar Energy Engineering-Transactions of the Asme*, 128(4), 487-497. <http://dx.doi.org/10.1115/1.2349550>
- Kaimal, J. C., Wyngaard, J. C., Izumi, Y., & Coté, O. R. (1972). Spectral characteristics of surface-layer turbulence. *Quarterly Journal of the Royal Meteorological Society*, 98(417), 563-589. <http://dx.doi.org/10.1002/qj.49709841707>
- Lopez, F., & Garcia, M. H. (2001). Mean flow and turbulence structure of open-channel flow through non-emergent vegetation. *Journal of Hydraulic Engineering-Asce*, 127(5), 392-402.
- Paulides, J. J. H., Encica, L., Jansen, J. W., Lomonova, E. A., & van Wijck, D. (2009). Small-scale urban venturi wind turbine: Direct-drive generator. *Proceedings IEEE International Electric Machines and Drives Conference, 2009. IEMDC '09, Miami, Florida*. <http://dx.doi.org/10.1002/10.1109/IEMDC.2009.5075381>
- Ragheb, M., & Ragheb, A. M. (2011). Wind Turbines Theory—The Betz Equation and Optimal Rotor Tip Speed Ratio. In R. Carriveau (Ed.), *Fundamental and Advanced Topics in Wind Power* (Chapter 2). USA: InTech. <http://dx.doi.org/10.5772/21398>
- Rotach, M. W. L., Vogt, R., Bernhofer, C., Batchvarova, E., Christen, A., Clappier, A., ... Voogt, J. A. (2005). BUBBLE—An urban boundary layer meteorology project. *Theoretical and Applied Climatology*, 81(3-4), 231-261. <http://dx.doi.org/10.1007/s00704-004-0117-9>
- Roth, M. (2000). Review of atmospheric turbulence over cities. *Quarterly Journal of the Royal Meteorological Society*, 126(564), 941-990. <http://dx.doi.org/10.1002/qj.49712656409>
- Sanz, C. (2003). A note on k-epsilon modelling of vegetation canopy air-flows. *Boundary-Layer Meteorology*, 108(1), 191-197. <http://dx.doi.org/10.1023/A:1023066012766>
- Stankovic, S., Campbell, N., & Harries, A. (2009). *Urban Wind Energy*. London: Sterling, VA: Earthscan.
- Stitt, F. A. (1999). *Ecological Design Handbook: Sustainable Strategies for Architecture, Landscape Architecture, Interior Design, and Planning*. New York: McGraw-Hill.
- Vermeer, L. J., Sorensen, J. N., & Crespo, A. (2003). Wind turbine wake aerodynamics. *Progress in Aerospace Sciences*, 39(6-7), 467-510. [http://dx.doi.org/10.1016/S0376-0421\(03\)00078-2](http://dx.doi.org/10.1016/S0376-0421(03)00078-2)
- Wahab, A. A., & Chong, W. T. (12-14 February 2003). Development of an indoor testing facility for low wind speed wind turbine research activities. *Proceedings of the 2nd Regional Conference on Energy Technology Towards a Clean Environment, Phuket, Thailand*.
- Wharton, S., & Lundquist, J. K. (2012). Atmospheric stability affects wind turbine power collection. *Environmental Research Letters*, 7(1), 014005.
- Yang, Z. F., Sarkar, P., & Hu, H. (2012). Visualization of the tip vortices in a wind turbine wake. *Journal of Visualization*, 15(1), 39-44. <http://dx.doi.org/10.1007/s12650-011-0112-z>
- Yusup, Y. (2012). Aerodynamic drag coefficient over equatorial coastal industrialized and urban areas. *Journal of Wind Engineering and Industrial Aerodynamics*, 110, 25-39. <http://dx.doi.org/10.1016/j.jweia.2012.07.006>
- Yusup, Y. B., Daud, W. R. W., Zaharim, A., & Talib, M. Z. M. (2008). Structure of the atmospheric surface layer over an industrialized equatorial area. *Atmospheric Research*, 90(1), 70-77. <http://dx.doi.org/10.1016/j.atmosres.2008.04.003>

Copyrights

Copyright for this article is retained by the author(s), with first publication rights granted to the journal.

This is an open-access article distributed under the terms and conditions of the Creative Commons Attribution license (<http://creativecommons.org/licenses/by/3.0/>).